Graphene in Cementitious Materials for Military Applications

Mine G. Ucak-Astarlioglu
Research Chemist, US Army Engineer Research and Development Center,
3909 Halls Ferry Road,
Vicksburg, MS 39180
USA

mine.g.ucak-astarlioglu@usace.army.mil

ABSTRACT

This research aims to develop novel cementitious materials to address the growing needs of improving logistical infrastructure for military applications. For that purpose, a two-dimensional (2D) material, graphene with superior mechanical, chemical, thermal, and electrical properties, is added into cement composites to enhance their internal matrix for advanced military applications. Upon selection of two different graphene resources, laboratory-generated (LGG)- and commercial-grade graphene (CGG) were obtained, and their optimum dispersion was determined by studying various graphene percentages in cement mixtures. Exploring chemical and physical interactions between graphene and its cementitious matrix through spectroscopic and microscopic techniques, composites' mechanical analyses completed using compression testing. Graphene-cement composites' microstructure/ processing/ property relationships were established and related to the compressive strength and longevity. This investigation showed the importance of graphene dispersion on the adhesion forces between cement's calcium silicate hydrate (CSH) gels and graphene surfaces. Analyses indicated that higher compressive strength graphene-cement mixtures have better microstructure patterns with much finer or reduced crack formation as observed qualitatively. Both LGG and CGG – cementitious composites showed a compressive strength increase over 7- to 28-day curing, and a stabilized minimal increase in 28 days compared to the reference materials without graphene. Morphologies of graphene-cementitious materials and their long-term durability are under investigation along with computational tools for materials design of graphene-cementitious composites.

This study establishes a baseline for understanding the influence of graphene in cementitious materials and presents a solid basis for the future development of graphene-cement mortar, and graphene-concrete composites leading to sustainable structures.

Keywords: Graphene, 2D materials, cement, paste, logistical, infrastructure, exfoliate, compressive strength.

1.0 INTRODUCTION

To meet the requirements of Army modernization priorities, innovative technologies are needed to deliver sustainable materials that provide resistance against harsh climate and external conditions while mitigating raw material shortages and supply issues. These advanced materials provide strategic readiness and protect valuable infrastructure components in military applications. Throughout the development of technologies to support our warfighters, working with greener systems has recently been emphasized. Graphene is one of these greener systems that can ultimately lessen demand for portland cement and thereby reduce CO_2 emissions from the portland cement manufacturing slowing down changes in climate [1]. Today, many international material and concrete organizations have a goal of manufacturing high-strength, high-durability, and low-permeability novel cementitious materials with little to zero CO_2 emission [2]. These

materials would also cut the overall maintenance costs due to aging and extreme weather conditions and increase the longevity of the infrastructure. Graphene owes its special properties to its sp^2 hybridized carbon atoms which form a covalent bond, and each carbon atom is connected to three other carbon atoms in its crystal lattice. Carbon atoms in graphene have a unique hexagonal arrangement that facilitates free mobility of electrons across the layers making this 2D material carry electrical charge or heat very effectively resulting in superior properties [3]. Graphene has unique tensile strength (130 GPa) and Young's modulus (1.1 TPa), respectively [4], [5].

Concrete shows deterioration through disintegration, erosion, reinforcement corrosion, delamination, spalling, alkali-aggregate reactions, and cracking. Asphalt pavements show deterioration over time (aging) resulting in cracking, potholes, and rough roads and runways. Graphene has the potential to greatly increase mechanical properties and longevity of infrastructure for moderate up-front cost. Further exploration of graphene in cementitious matrices will facilitate adoption of graphene for military infrastructure, proving these studies invaluable for military programs and warfighter support.

2.0 EXPERIMENTAL APPROACH

2.1 Selection of Graphene Material and Dispersant

Two types of graphene-related materials (GRM), graphite and graphene, were used in the preparation of graphene-cement mixtures. Cost, ease of dispersion, and mechanical performance were used as the selection criteria for the GRM. Results from graphene-cement mixtures were compared to the reference mixtures that contained no graphene. Graphite grade BF-103 was purchased from Barite World (BW) for $0.025 per gram. Commercially available graphene nanoplatelet, xGnP® grade C-750 was purchased from XG-Sciences® for $1 per gram. These GRM have significantly different particle sizes as reported by their manufacturers: xGnP® C-750 has less than 2 μm, and BF-103 has 4.6 to 27.2 μm particle size range. GRM surface areas were determined at the U.S. Army Engineer Research and Development Center (ERDC) using an Autosorb Brunauer-Emmett-Teller (BET) instrument. Surface areas were found as 1 m^2/g for BF-103 and 750 m^2/g for xGnP® C-750, respectively. GRM particle sizes and surface areas may significantly affect the microstructural and mechanical properties of graphene-composites [5].

To produce LGG, an exfoliation method was used to convert BF-103 graphite into graphene through high shear rate mixing [6]. Scanning electron microscopy and Raman spectroscopy were used to compare the raw graphite material to the exfoliated material to ensure that the graphene material was successfully obtained through exfoliation method to be used in this research. Dispersion of the GRM in the cementitious environment was found to be the most common obstacle in in the literature [6]. For this purpose, two high range water reducing admixtures (HRWRA or dispersant), MasterGlenium 7920 from Master Builders Solutions, and ADVA®198 from GCP Applied Technologies were tested to achieve the highest dispersion of graphene in the aqueous solution. Based on the zeta potential analyses and visual inspection of graphene dispersion over time, MasterGlenium 7920 HRWRA was found to perform better than the ADVA®198 in graphene dispersion and used in this study.

2.1.1 Aqueous Suspension

To obtain a stabilized aqueous solution, water, and a predetermined optimum dose of HRWRA were stirred magnetically until complete solubilization of dispersant. Then adding the graphene into this mixture, solution was sonicated using a QSonica sonicator for two minutes. The sonicator creates shock waves to provide high enough energy to break the inter-layer van der Waals bonds in graphite [7]. Figure 1 shows the interaction of dispersant polycarboxylate molecule with stacks of graphene.

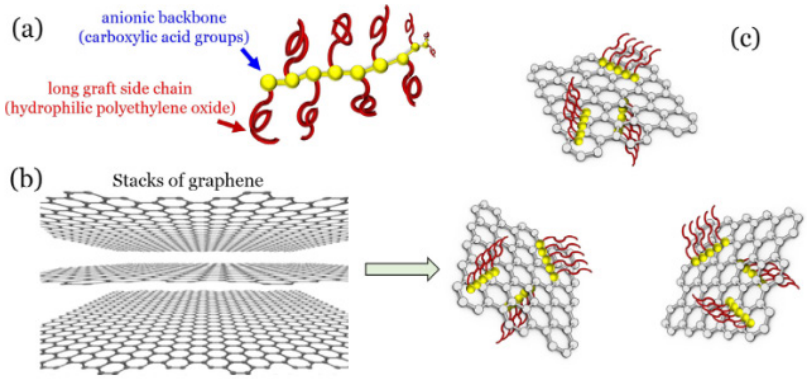

Figure 1: Graphene interaction with dispersant. Dispersant, b) stacks of graphene, and c) interaction of dispersant and graphene [7].

2.2 Preparing Graphene-Cement Mixtures – High-Shear-Rate Mixer

Stabilized aqueous graphene dispersant solution was placed into a Waring Commercial MX1300XTX 3.5-hp high-shear-rate mixer at the rate of 5,000 rpm for 20 minu. High shear exfoliation uses shear forces to separate the graphene sheets [9]. Next, this solution was placed into a Hobart mixing bowl, and the portland cement was added. After mixing at a slow speed of 140 ± 5 rpm for 60 seconds, the mixer was stopped for 30 seconds to scrape down the paste collected on the sides of the bowl, and mixing continued at medium speed (285 ± 10 rpm) for 10 minutes. The impact of HRWRA on the graphene dispersion and performance of graphene-cement mixture were investigated. Figure 2 shows the graphene-cement paste preparation.

Figure 2: Graphene-cement mixture preparation from left to right are: High shear rate mixer and Hobart bowl; aqueous dispersed graphene solution; graphene-cement paste in Hobart mixer; cube and cylinder molds with graphene-cement paste.

2.3 Preparation of Graphene-Cement Mixtures – Proportions

In mixtures, Type I/II portland cement was used in meeting the requirements of ASTM C150/C150M-19 [8] that was sourced from Holcim USA's St. Genevieve, Missouri. Table 1 shows LGG-cement mixture proportions, where m is mass and w/c is the water to cement ratio. The MasterGlenium 7920 HRWRA used was 2.26% by mass of cement. Graphene % shows the graphene to cement ratio by weight. Using tap water, the water-to-cement ratio (w/c) was kept constant at w/c = 0.25.

Table 2 shows CGG-cement mixture proportions. HRWRA dosage was based onto the graphene amount used and determined as a 1.84 factor of graphene (w/w). Graphene % shows the graphene to cement ratio by weight. Using tap water, w/c = 0.4 was held constant.

Table 1: Mixture proportions for graphene-cement paste made from LGG.

Graphene%	m_{HRWRA} (lb)	w/c	m_{cement} (lb)	$m_{graphite}$ (lb)	$m_{water,mix}$ (lb)
Reference	0.69	0.25	30.90	0.00	7.72
0.02%	0. 69	0.25	30.90	0.01	7.72
0.05%	0. 69	0.25	30.89	0.02	7.72
0.21%	0. 69	0.25	30.85	0.06	7.71
0.62%	0. 69	0.25	30.75	0.20	7.69
2.08%	0.69	0.25	30.41	0.60	7.60

Table 2: Mixture proportions for graphene-cement paste made from CGG.

Graphene%	m_{HRWRA} (lb)	w/c	m_{cement} (lbm)	$m_{graphene}$ (lbm)	$m_{water,mix}$ (lbm)
Reference	0.0000	0.40	7.57	0.00	3.03
0.3%	0.01	0.40	7.55	0.02	3.01
0.6%	0.02	0.40	7.53	0.05	3.00
0.9%	0.04	0.40	7.52	0.07	2.98

2.4 Cube and Cylinder Preparation for Curing Process

The graphene-cement paste was cast into nine 2-in.-diameter by 4-in.-tall plastic cylindrical molds and three 1-in. cubical stainless-steel molds. External vibration was applied to cylinders and cubes. After casting, the paste that had been forced out onto the tops of the molds was smoothed with a trowel. The specimens were moist cured in a fog room until 7-, 14-, or 28-day age. The methods prescribed in ASTM C1856/C1856M-17 [9] were used to measure the flow of the mixture by filling the conical mold in one lift, removing it, and allowing the mixture to spread for 2 minutes, measuring two diameters, and taking the average.

2.5 Mechanical Testing - Unconfined Compressive Strength Test

The same constant load rate was applied to all specimens during this research based onto the ASTM C109/C109M-21 [10] standard for cube tests. The average of three test results were taken as the representative compressive strength. Before and after pictures of an unconfined compressive strength test for the 0.02% LGG cement mixture are shown in Figure 3, respectively.

Before the application of load | After the application of load

Figure 3: Before and after pictures of an unconfined compressive strength test for 0.02% LGG-based cement mixture.

2.6 Chemical and Microstructure Analyses

2.6.1 X-ray Photoelectron Spectroscopy (XPS) Analyses

All XPS data were collected using a PHI Quantera SXM Scanning X-Ray Microprobe with a base pressure of 5×10^{-9} torr. Survey spectra were recorded using 0.5-eV step sizes with a pass energy of 140 eV. Elemental spectra were recorded using 0.1-eV step sizes with a pass energy of 26 eV. Spectra were not corrected to 284.5 eV or Shirley baseline subtracted. XPS allows quantitative analysis of elemental content and binding at the material surface. Figure 4 shows the XPS spectra of xGnP® grade C-750 and BF-103, and Table 3 shows their atomic content in percentage.

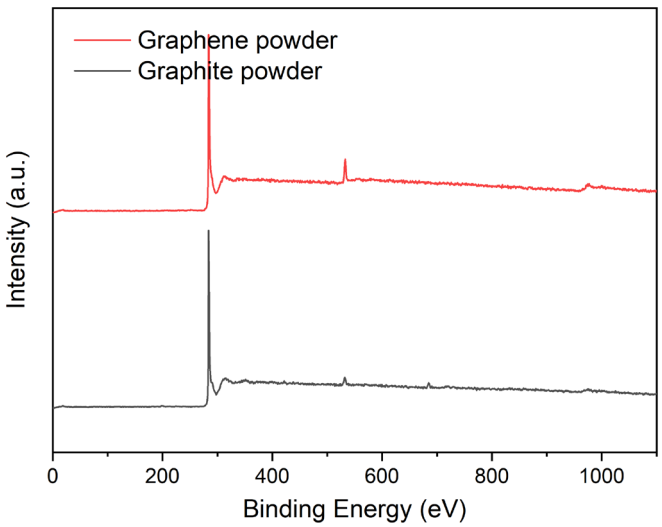

Figure 4: XPS spectra of xGnP® grade C-750 and BF-103.

Graphene and graphite samples show high carbon content and some surface oxygen content. The high-resolution scans of the C1s (tall peaks) and O1s (short peaks) regions can be used to give a better understanding of the interactions taking place at the exposed surface of the ground samples. Based on the XPS results, more oxygen content was found in the xGnP©C-750 graphene compared to BA graphite.

Table 3: XPS survey spectra – % atomic content summary.

Graphene Material	% Atomic Content						
	C	O	Si	N	Al	Cl	F
BA Graphite Powder	95.1	2.7	-	-	-	-	2.2
xGnP© C-750 Sciences Graphene Powder	93.8	6.2	-	-	-	-	-

2.6.2 Raman Analysis

All Raman spectra were collected using a Renishaw inVia Raman microscope outfitted with a 5-mW, 532-nm laser using a 50x objective lens. High-resolution single Raman spectra were collected and used for Lorentzian peak fitting. Because cement has high amounts of background fluorescence, a MatLab script was used to subtract the background in processing the raw data.

2.6.3 Powder X-Ray Diffraction (XRD)

All powder XRD patterns were collected using a Rigaku SmartLab II using zero background sample holders at a scan rate of 8 º2θ /min and a 0.015 º2θ step size.

2.6.4 Fourier-Transform Infrared Spectroscopy (FTIR) Analysis

All FTIR spectra were collected using a Nicolet FTIR microscope with a liquid nitrogen-cooled detector. An attenuated total reflection (ATR) attachment was used to collect data from the surface of the cement composite samples. A background was collected before each sample was collected. FTIR showed peaks for carbonates at 870 cm^{-1}, Si-O stretching at 961 cm^{-1}, and two broad overlapping peaks at 1,390 cm^{-1} and 1,490 cm^{-1} that can also be attributed to the carbonates present in the cement.

2.6.5 Scanning Electron Microscopy (SEM)/Energy-Dispersive X-Ray Spectroscopy (EDS) Analyses

SEM was performed using a FEI Nova NanoSEM 630 under low vacuum at pressures of 0.1 to 0.5 mbar and an accelerating voltage of 15kV. A backscattered electron detector or low voltage-high contrast detector (VCD) was used collecting all images. Imaging was performed in multiple locations on each sample to observe an accurate representation. EDS was used in conjunction with SEM imaging to perform chemical microanalysis of a specimen and performed using a Bruker Quantax AXS detector, which attached directly to the SEM. This analysis can focus data collection to a single point or the entire field of view. EDS mapping assigns colours to the area's constituents to aid in differentiation. The software can output collected data in many ways including atomic percentages, major oxides, or individual elements.

3.0 RESULTS AND DISCUSSION

3.1 Compressive Strength

The averaged and maximum compressive strength versus curing days for LGG- and CGG-cement

composites were compared to their original cement paste references as shown in Figure 5 and Figure 7, respectively. Their normalized compressive strength, $r_{strength}$, versus curing are shown in Figure 6 and Figure 8, respectively. Figure 5 and Figure 7 indicate a significant increase in the averaged compressive strength for 7- and 14-day curing compared to the reference. Among all, the lowest LGG amounts (0.05%, and 0.02%) presented the highest compressive strength increase relative to the other proportions of LGG and CGG-cement pastes. Error bars are shown for LGG-cement composites, where averaged compressive strengths were presented. Figure 6 and Figure 8 show that for CGG-cement paste, compressive strengths start to level off after 14 days for almost all amounts, except for the lowest, 0.3% graphene-cement paste, which shows an increase in compressive strength on all curing days. On the other hand, at 28-day curing, the increase in compressive strength decreases for the highest loadings. Figure 6 shows that the lowest graphene loaded (0.02%) paste shows stabilized increase in the compressive strength at 28 days. However, after 14 days of curing, the LGG-paste samples did not offer significant improvement over the reference and in two samples the compressive strength diminished considerably. These compressive strength improvements substantiated the conclusion that graphene can significantly affect and accelerate the cement hydration process due to the nucleation effect. Additionally, the optimum dose of GRM is important in obtaining the highest compression strength possibly due to water graphene agglomeration at higher dosages.

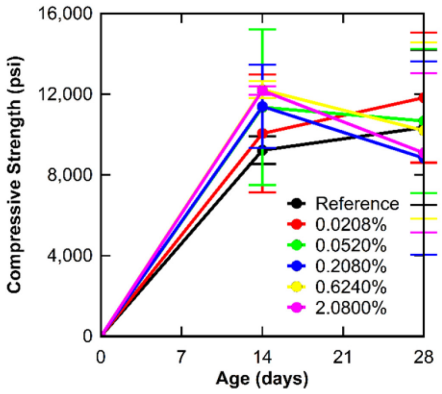

Figure 5: Average compressive strength of LGG-based cement pastes.

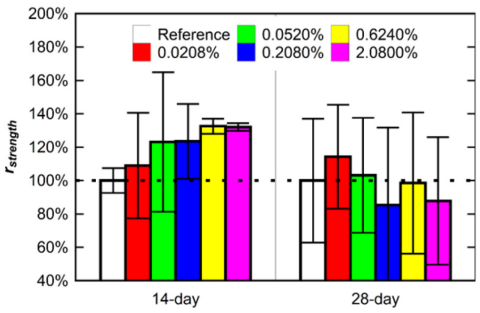

Figure 6: Normalized average compressive strength of LGG-based graphite-cement pastes.

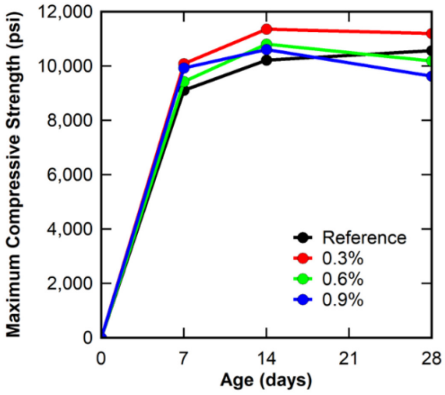

Figure 7: Maximum compressive strength of CGG-based cement paste.

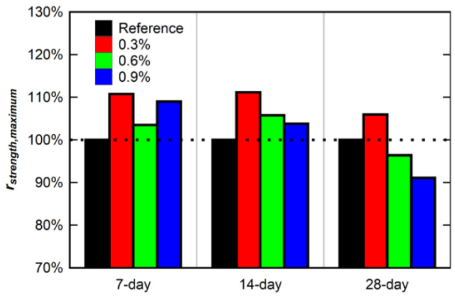

Figure 8: Normalized maximum compressive strength of CGG-based graphite-cement pastes.

LGG- and CGG-based cement pastes provided higher compressive strength than the reference paste at 7- and 14-day curing. However, after 14 days, the increase in the compressive strength becomes minimal for LGG-cement pastes and seems to stabilize for CGG-cement pastes. In addition, 0.3% CGG-cement paste shows an increase in the compressive strength from seven to 28 days. This noted strength increase in 7-, 14-, 28-day curing provides an opportunity for the use of graphene-composites in numerous applications.

3.2 Chemical and Microstructure Tests and Results

In the chemical investigation of graphene-cement paste, XPS, XRD, FTIR, and Raman spectroscopy were used. For microstructure analyses, SEM/ EDS was used. Raman spectra in the investigation of dispersant effect (on the left) and the graphene amounts used in the graphene-cement pastes (on the right) are shown in Figure 9.

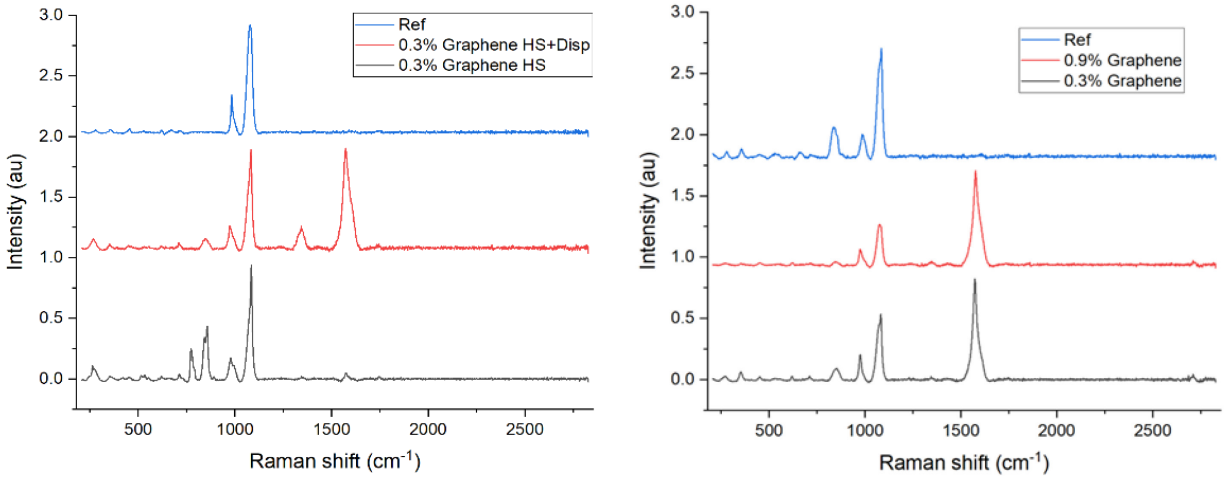

With/ without dispersant **With different graphene amounts**

Figure 9: Raman spectra of reference- and 0.3% graphene-cement paste with and without dispersant (left) and with 0.9% CGG cement paste (right).

Figure 9 shows the Raman spectroscopic investigation on the effect of dispersant (on the left) and the graphene amounts used in the cement pastes (on the right) and compares the findings to the reference paste. Disp represents HRWRA and HS high shear rate in the labels. D, G, and 2D peaks were in the graphene containing samples. Similarly, reference samples also presented some peaks close to these D, G and 2D peak locations. Although reference sample peaks were not easily identifiable in the literature, they were differentiated from the peaks resulting from graphene due to their decreased intensity, not sharing the same intensity ratio as the graphene has and having slightly different Raman shifts. In the figure on the left, the G peak in the graphene containing samples is centered at ~1575 cm^{-1}, whereas the unknown peaks in the cement control samples is centered at ~1595 cm^{-1}. However, these unknown peaks innate to the cement matrix material do clearly cause some peak broadening of the D, G and 2D peaks, which increase the full width at half maximum (FWHM) of these peaks. Peaks occurring below ~1340 cm^{-1} originate from the cement matrix material, a mixture of crystalline oxides and carbonates. The most intense peak, centered at 1084 cm^{-1}, likely results from the carbonate stretching.

The visual inspection of LGG cement pastes showed a white colour calcite formation as presented in Figure 10 at the lower graphene amounts.

Figure 10: LGG- based cement cubes obtained from 0.02% (w/w) to 0.62% (w/w).

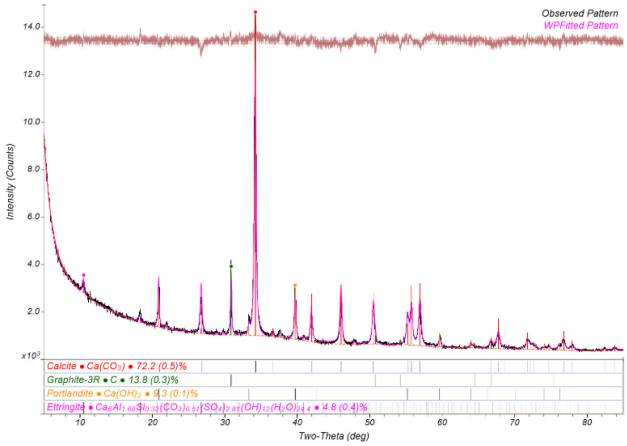

Figure 11: XRD of white side of 0.05% LGG-based cement paste cube.

Figure 11 shows the XRD chromatography investigation on the white colour calcite site of the graphene-cement cube with 0.05% LGG amounts, and Figure 12 presents the chemical composition distribution. XRD analyses showed remaining hydration products as portlandite, ettringite, and graphite.

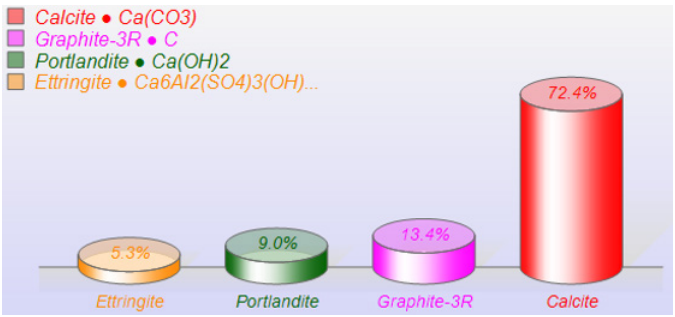

Figure 12: XRD of white side of 0.05% LGG-based cement paste hydration product distribution.

The white coloured calcite formation was also investigated using visual and SEM/EDS analyses. It was observed that the top faces of all these cubes – in direct contact with air, and/ or possibly due to the moisture in the air in the fog room – presented a high percentage of calcite formation. This observation, when compared to the samples with higher amounts of LGG and CGG, in which minimal to no calcite formation was observed, points out the importance of HRWRA dosage used in the preparation of graphene cement paste. LGG-cement pastes were prepared with a higher dosage of HRWRA compared to the CGG-cement-pastes.

Polished graphene-cement mixtures were analysed using a high-resolution SEM. Light grey (dehydrated cement) and dark grey (hydrated cement) zones presented similar elemental composition (mostly calcium and silicon with trace amounts of other ions); although had different visual appearances. The black region presented predominantly carbon. Figure 13 shows that addition of graphene into cement matrix refines the total morphology/ porosity of the paste as graphene acts as a nano-filler into filling the matrix system [11]. It was observed that graphene with larger specific surface area can facilitate early cement hydration reactions due to nucleation that leads to a more compacted and refined matrix. However, going from 0.3% to 0.9% graphene amount, agglomeration of graphene and reduced nano-filler effect of graphene in the cement composites, and resulted in reduced compressive strength.

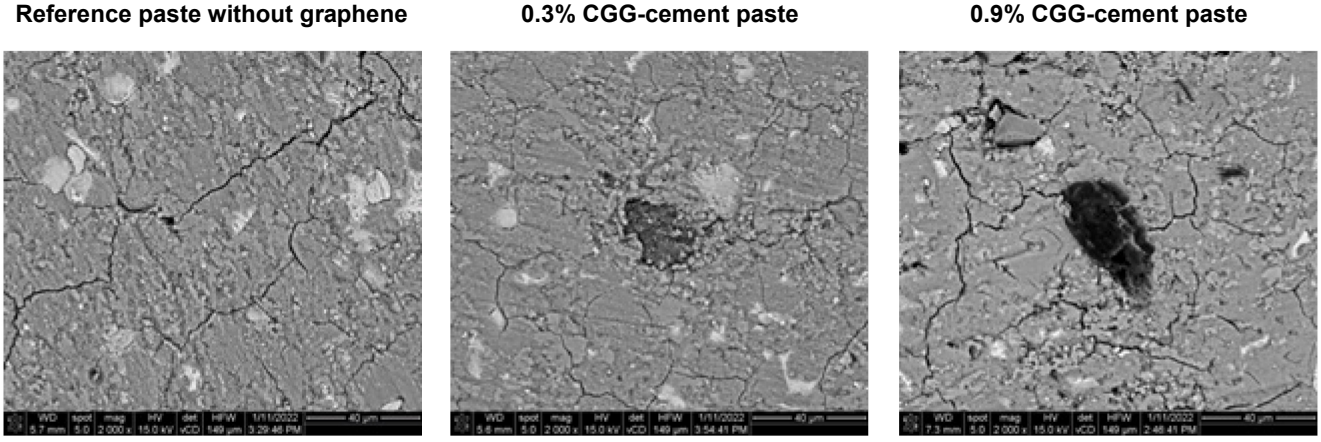

Figure 13: Reference, 0.3% CGG, and 0.9% CGG-cement paste at 2,000x magnification.

SEM/EDS analysis was also used for elemental mapping in the circled area as shown in Figure 14, and each element presented with a different colour. EDS elemental composition for 0.3% CGG based-cement paste with mass and atomic concentration percentages was presented in Table 4. These measurements confirmed the presence of graphene in the cement paste samples and their integration into cement.

Based on the SEM microstructural analyses, higher compressive strength graphene-cement mixtures were found to have better microstructure patterns with much finer or reduced crack formation as observed qualitatively. SEM images show that in the composite matrices, cracks are stopped in the presence of graphene sheet, whereas in ordinary matrices cracks seem to continue in the form of a straight line.

Knowledge of optimum dosage is imperative to prevent agglomerations. In cement mixture preparations when the dosage is above a certain threshold, agglomeration occurs and causes many layers of graphene to come together and form multi layers of graphene. As a result of these multi layers, and weak van der Waals interactions, friction force between graphene and cementitious material is reduced and results in debonding and displacement of layers that reduces the strength of graphene-cement mixtures.

SEM/EDS image Circled area

EDS map - chemical microstructure analysis

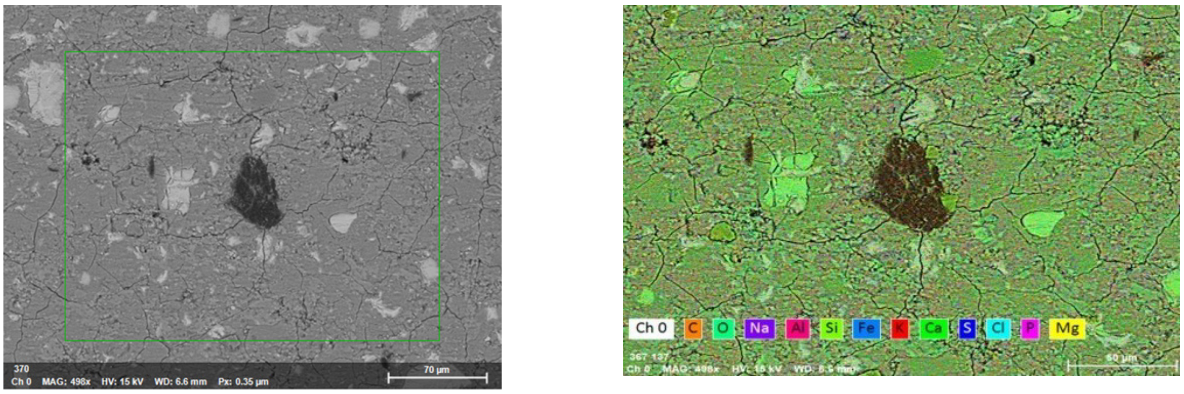

Figure 14: SEM/EDS image and chemical microstructure analysis of 0.3% CGG-based cement paste at 498x magnification.

Table 4: EDS Elemental composition for CGG-based cement paste with 0.3% graphene-loading.

Element	Atomic Number	Netto	Mass [%]	Mass Norm [%]	Atom [%]	Abs. Error [%]	Rel. Error [%]
Oxygen	8	241099	13.51	49.77	59.61	1.49	11.00
Calcium	20	448342	4.40	16.21	7.75	0.16	3.54
Silicon	14	219237	3.95	14.55	9.93	0.19	4.79
Carbon	6	42197	2.56	9.44	15.07	0.33	12.92
Sodium	11	32613	0.95	3.51	2.92	0.08	8.88
Aluminum	13	43119	0.82	3.03	2.15	0.06	7.72
Magnesium	12	32307	0.70	2.58	2.03	0.06	8.92
Sulfur	16	11921	0.25	0.91	0.55	0.03	13.79
Iron	26	0	0.00	0.00	0.00	0.00	0.920
		Sum	27.14	100.00	100.00		

4.0 CONCLUSIONS AND RECOMMENDATIONS

Our research demonstrates that it is possible to obtain graphene-cement pastes with higher compressive strength compared to their reference pastes. Additionally, in another study we found that asphalt aging can be significantly improved by the addition of GnPs in the graphene-asphalt composites [12]. Exfoliation of graphite proved to be a viable technique in the fabrication of graphene. Graphene-cement pastes were prepared from LGG and CGG with ASTM Type I/II portland cement. Including graphene in the cement mix resulted in higher early compressive strength. However, the results also indicated that, there is an optimum value for the graphene amount that can be added to the cement matrix, and higher than this amount can reduce the long-term compressive strength in the cement pastes. Particle size and surface area of graphene, shear rate, and dispersant had profound effects on agglomeration. Effective graphene dispersion was achieved when the graphene particle size was less than 2 µm with a surface area of 750 m^2/g for xGnP® C-750, and 4.6 to 27.2 µm particle size range with a surface area of 1 m^2/g for BF-103, where shear rate was kept at 5,000 rpm. XPS, XRD, Raman, SEM/EDS analyses were used to determine the composites' chemical

structure and microstructure. These properties along with the mechanical strength were used to map graphene-cement paste structure/processing/property relationships. Graphene dispersion was found to control the adhesion forces between CSH gels and the graphene particle surfaces. LGG- and CGG-based graphene cement mixtures showed an increase in the compressive strength over 7-, 14-, and 28-day curing periods at optimum graphene amounts. Preliminary dispersion studies indicated that MasterGlenium 7920 was the most effective HRWRA for graphene dispersion. EDS elemental mapping confirmed the successful incorporation of graphene into the cement paste. Additionally, EDS indicated that the higher the amount of dispersant, the more calcite formation occurs at lower LGG percentages.

In the future, the fabrication and mechanical strength of graphene-cementitious materials, specifically graphene-mortar and -concrete composites will continue to be studied with the addition of fine and coarse aggregates, respectively. The relationship between the graphene and hydration products will be further explored. Morphologies of graphene-cementitious materials and their long-term durability will be studied along with computational tools for materials design of graphene-cement composites. We expect to see significant improvements in graphene-concrete over conventional concrete in tensile and flexural applications where the tensile strength and Young's modulus of graphene will be utilized better.

Exploring the opportunities in the use of graphene, we will obtain better performing structures in military engineering under blast and penetration situations. Further investigation of graphene in cementitious matrices will facilitate adoption of GRM for military construction, warfighter support, fighting climate change, and use in our nation's vast civil works infrastructure.

5.0 ACKNOWLEDGEMENTS

The authors would like to thank the 6.3 Military Engineering Graphene for Military Applications Program for funding.

6.0 REFERENCES

[1] Felipe Basquiroto de Souza, Xupei Yao, Wenchao Gao, and Wenhui Duan, "Graphene opens pathways to a carbon-neutral cement industry," Science Bulletin, vol. 67, no. 1, pp. 5–8, 2022.

[2] G. Habert et al., "Environmental impacts and decarbonization strategies in the cement and concrete industries," Nature Reviews Earth & Environment volume, vol. 1, pp. 559–573, 2020.

[3] Y. W. Sun et al., "Mechanical properties of graphene," Applied Physics Reviews, vol. 8, no. 021310, 2021.

[4] Ivan Vlassiouk et al., "Strong and Electrically Conductive Graphene-Based Composite Fibers and Laminates," ACS Appl. Mater. Interfaces, vol. 7, pp. 10702–10709, 2015.

[5] Youli Lin and Hongjian Du, "Graphene reinforced cement composites: A review," Construction and Building Materials, vol. 265, pp. 1–16, 2020.

[6] Dimitar Dimov et al., "Ultrahigh Performance Nanoengineered Graphene–Concrete Composites for Multifunctional Applications," Advanced Functional Materials, vol. 28, p. 1705183, 2018.

[7] H. Du and S. Dai Pang, "Dispersion and Stability of Graphene Nanoplatalet in Water and Its Influence on Cement Composites," Construction Building Materials, vol. 167, pp. 403–413, 2018.

[8] ASTM C150/C150M-19 Standard Specification for Portland Cement. West Conshohocken, PA: ASTM International, 2019.

[9] ASTM C1856/C1856M-17 Standard Practice for Fabricating and Testing Specimens of Ultra-High Performance Concrete. West Conshohocken, PA: ASTM International., 2017.

[10] ASTM C109/C109M-21 Standard Test Method for Compressive Strength of Hydraulic Cement Mortars (Using 2-in. or [50 mm] Cube Specimens). West Conshohocken, PA: ASTM International, 2021.

[11] Małgorzata Krystek et al., "High-Performance Graphene-Based Cementitious Composites," Advanced Science, vol. 6, no. 9, p. 1801195, 2019.

[12] Chris S. Griggs, Sarah G. Zetterholm, Mine G. Ucak-Astarlioglu, Jesse D. Doyle, and Luke Gurtowski, "Targeted Opportunities for Graphene Enhanced Water Security and Infrastructure Materials," in Research Specialist Meeting, London, England, May 2023.

7.0 AUTHOR BIOGRAPHY

Dr. Mine Ucak-Astarlioglu is a Research Chemist at the Concrete Materials Branch (CMB), Geotechnical and Structures Laboratory (GSL), U.S. Army Engineer Research and Development Center (ERDC) in Vicksburg, Mississippi. Dr. Ucak-Astarlioglu is experienced in physical organic chemistry and materials science. Her research includes graphene in cementitious and advanced materials.